ELSEVIER

Materials Science and Engineering A238 (1997) 78–84

MATERIALS SCIENCE & ENGINEERING A

# Effect of grain boundary width on grain growth in a diffuse-interface field model

Danan Fan [a,*], Long-Qing Chen [b], S.P. Chen [a]

[a] *Theoretical Division, MS B262, Los Alamos National Laboratory, Los Alamos, NM 87545, USA*
[b] *Department of Materials Science and Engineering, The Pennsylvania State University, University Park, PA 16862, USA*

**Abstract**

The effect of grain boundary width on grain growth in the diffuse-interface field model is studied by analytical formulations and computer simulations. It has been shown that the grain growth kinetics will be slowed down if the number of grid points is insufficient to resolve the grain boundaries. When there are more then seven grid points in grain boundary regions, the grain growth is independent of the grain boundary width and the motion of a diffuse grain boundary is identical to its sharp-interface limit. The moments of grain side distributions reach stable values in the dynamically scaling regime and they are independent of the grain boundary width. It has been shown that, in addition to lattice anisotropy, coalescence affect the topological distributions. © 1997 Elsevier Science S.A.

*Keywords:* Grain boundary width; Diffuse-interface field; Grain growth

## 1. Introduction

Normal grain growth in single phase materials is a process of grain boundary migration, driven by mean curvatures of grain boundaries, to reduce the total amount of grain boundary energy or grain boundary area. Most of previous mean-field and statistical theories as well as computer simulation models for grain growth were reviewed by Atkinson [1], Glazier [2] and Fradkov [3]. All these models assume sharp grain boundaries, which are abstract geometrical surfaces possessing properties such as area, curvature, free energy and mobility. Due to the difficulty of directly incorporating topological features into analytical theories of grain growth, the Potts model [4–10] simulations and the evolution of soap froth [11–14] have been extensively employed to study the kinetics and topological features of grain growth. While most Potts model grain growth simulation results agree with those of a soap froth, the Potts model simulations consistently predicted wider side and grain area distributions than the soap froth [11]. Holm et al. [10] showed that the lattice anisotropy introduced by the discrete lattice in the Potts model is responsible for the deviation of distributions from the soap froth. In the low lattice anisotropy Potts model simulations, the moments of distributions are very close to those obtained from the evolution of soap froth [10].

Recently, we proposed a rather different model for investigating grain growth kinetics [15–18]. A key new feature of this model is that the grain boundaries are diffuse with a finite thickness, similar to the theoretical treatment of antiphase domain boundaries by Allen and Cahn [19]. The grain boundary energy is introduced through the gradient energy terms in the free energy functional. One of the main advantages of this model is that any arbitrary microstructure can be easily treated since the interfaces are not singular surfaces requiring imposition of moving boundary conditions as in the sharp-interface description. Another feature of this model is that the anisotropy associated with discretizing the microstructure is almost non-existent as long as there are enough grid points to resolve the grain boundary regions [15,20]. Surprisingly, the moments of distributions obtained from this model are similar to those from Potts model simulations with high lattice anisotropy rather than those from soap froth [16]. These results suggest that there are effects, other than lattice anisotropy, which contribute to the discrepancies between the results of simulations and soap froth. In

* Corresponding author.


*PII* S0921-5093(97)00437-1

this paper, we study the effect of grain boundary width on the grain growth kinetics and distributions in this diffuse-interface field model.

## 2. Diffuse-interface field model

In the diffuse-interface field model [15,17], an arbitrary polycrystalline microstructure is described by a set of continuous field variables,

$$\eta_1(r), \eta_2(r), \ldots, \eta_p(r)$$

where $p$ is the number of possible orientations in space and $\eta_i$ ($i = 1, \ldots, p$) are called orientation field variables which distinguish the different orientations of grains and are continuous in space. $r$ is the position in the space. Their values continuously vary from $-1.0$ to 1.0. In real materials, the number of orientations is infinite ($p = \infty$). However, it was shown that a finite number of $p$ ($p > 30$) might be sufficient to realistically simulate grain growth [15].

Within the diffuse interface theory [21], the total free energy of an inhomogeneous system can be written as:

$$F = \int \left[ f_0(\eta_1(r), \eta_2(r), \ldots, \eta_p(r)) + \sum_{i=1}^{p} \frac{\kappa_i}{2} (\nabla \eta_i(r))^2 \right] \mathrm{d}^3 r \tag{1}$$

where $f_0$ is the local free energy density which is a function of field variables $\eta_i$, and $\kappa_i$ are the gradient energy coefficients. Grain boundary energy is introduced by the gradient terms $(\nabla \eta_i)^2$ in Eq. (1). The smaller the gradient energy coefficient $\kappa_i$ is, the thinner the boundary region. If all the gradient energy coefficients go to zero, the boundary thickness becomes infinitely thin, i.e. a sharp interface.

The spatial and temporal evolution of orientation field variables is described by Ginzburg-Landau equations:

$$\frac{\mathrm{d}\eta_i(r, t)}{\mathrm{d}t} = -L_i \frac{\delta F}{\delta \eta_i(r, t)} = -L_i \left( \frac{\partial f_0}{\partial \eta_i} - \kappa_i \nabla^2 \eta_i \right)$$
$$i = 1, 2, \ldots, p \tag{2}$$

where $L_i$ are the kinetic coefficients related to grain boundary mobility, $t$ is time and $F$ is total free energy given in Eq. (1).

To simulate grain growth kinetics, we assumed the following simple free energy density functional,

$$f_0(\eta_1, \eta_2, \ldots, \eta_p) = \sum_{i=1}^{p} \left( -\frac{\alpha}{2} \eta_i^2 + \frac{\beta}{4} \eta_i^4 \right) + \gamma \sum_{i=1}^{p} \sum_{j \neq i}^{p} \eta_i^2 \eta_j^2 \tag{3}$$

where $\alpha$, $\beta$ and $\gamma$ are phenomenological parameters. The main requirement for $f_0$ in modeling grain growth for a pure single-phase is that it has $p$ degenerate minima, $f_{\min}$, located at $(\eta_1, \eta_2, \ldots, \eta_p) = (1, 0, \ldots, 0)$, $(0, 1, \ldots, 0)$, $\ldots$, $(0, 0, \ldots, 1)$ in $p$-dimensions space. It can be shown that, if $\gamma > \beta/2$, Eq. (3) gives $2p$ potential minima (wells) in the $p$-field space, which represent the equilibrium free energies of crystalline grains in $2p$ different orientations.

In the computer simulation, Eq. (2) are discretized in space and time. The Laplacian is discretized by the following equation:

$$\nabla^2 \eta_i = \frac{1}{(\Delta x)^2} \left[ \frac{1}{2} \sum_j (\eta_j - \eta_i) + \frac{1}{4} \sum_k (\eta_k - \eta_i) \right] \tag{4}$$

where $\Delta x$ is the grid size, $j$ represents the first-nearest neighbors of site $i$ and $k$ represents the second-nearest neighbors of site $i$. For discretization with respect to time, the explicit Euler equation is used:

$$\eta_i(t + \Delta t) = \eta_i(t) + \frac{\mathrm{d}\eta_i}{\mathrm{d}t} \times \Delta t \tag{5}$$

where $\Delta t$ is the time step for integration.

## 3. Motion of a grain boundary

In the diffuse-interface field model, a grain, with an arbitrary orientation in space, is described by a continuous field variable $\eta(r)$ and hence a grain boundary separating two grains can be described by two field variables, $\eta_1(r)$ and $\eta_2(r)$. The energy of a flat grain boundary between grain 1 and 2, $\sigma_{gb}$, can be calculated as

$$\sigma_{gb} = \int_{-\infty}^{+\infty} \left[ \Delta f_0(\eta_1, \eta_2) + \frac{\kappa_1}{2} \left( \frac{\mathrm{d}\eta_1}{\mathrm{d}x} \right)^2 + \frac{\kappa_2}{2} \left( \frac{\mathrm{d}\eta_2}{\mathrm{d}x} \right)^2 \right] \mathrm{d}x \tag{6}$$

where $\Delta f_0(\eta_1, \eta_2)$ is the excess free energy density of an inhomogeneous system over an homogeneous system with equilibrium values of $\eta_1(r)$ and $\eta_2(r)$. For a flat boundary and for $\kappa_1 = \kappa_2 = \kappa$, it can be easily shown that [19,20], grain boundary width ($l$) in this model varies as,

$$l = \eta_{eq} \left( \frac{\kappa}{\Delta f_0} \right)^{1/2} \tag{7}$$

where $\eta_{eq}$ is the equilibrium value of the orientation variable.

It has been shown that [20,22], for the particular case of a circular grain embedded in another grain with the condition that the grain size is much larger than the grain boundary width (sharp grain boundary condition), the kinetics of the circular grain follows:

$$R_0^2 - R^2 = 2L\kappa t \tag{8}$$

where $R_0$ is the original radius of the circular grain, $R$ is the radius at time $t$ and $L_1 = L_2 = L$, which gives an isotropic grain boundary mobility condition.

According to Eq. (8) and Eq. (7), the kinetics (velocity) of a grain boundary with isotropic grain boundary energy is only dependent on the coefficients $\kappa_i$ and $L_i$, but not on $\Delta f_0$, whereas its thickness and grain boundary energy vary with $\kappa_i$ and $\Delta f_0$. Therefore, varying $\Delta f_0$, while keeping $\kappa_i$ and $L_i$ constant, will change the boundary energy and thickness but not its velocity. However, Eq. (8) was derived based on the assumption that the grain size is much larger than the boundary width [20,22], i.e., the sharp-interface limit. Meanwhile, in computer simulation of grain growth using a uniform grid for discretizing the differential Eq. (2), the condition, $R \gg l$, is usually not satisfied. Therefore, it is important to understand the relationship between the numerical simulation based on the diffuse-interface description and its sharp-interface limit.

To simulate the grain boundary motion, we consider a circular grain ($\eta_1$) embedded in another grain ($\eta_2$) (Fig. 1). We employed $200 \times 200$ square lattice points to spatially discretize the kinetic equations with periodic boundary conditions applied along both Cartesian coordinate axes. The discretizing grid size $\Delta x$ is chosen to be 2.0 and the time step $\Delta t$ is 0.25. The initial radius of the circular grain was chosen to have 120 grid points in diameter, which is much greater than the width of the grain boundary. We consider the case: $\kappa_1 = \kappa_2 = \kappa = 2.0$ and $L_1 = L_2 = L = 1.0$, which give an isotropic grain boundary energy and isotropic grain boundary mobility, respectively. For the local free energy density function, the following initial parameters were assumed: $\alpha = 1.0$, $\beta = 1.0$ and $\gamma = 1.0$. To vary $\Delta f_0$, the local free energy density function $f_0$ was multiplied by a coefficient $\mu$. The width and energy of the grain boundary vary with $\mu$ while the velocity in the sharp-interface limit should not be affected.

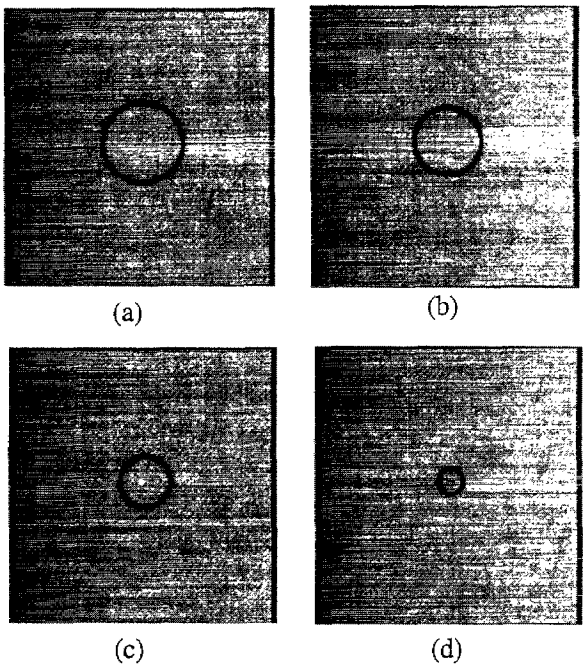


Fig. 1. The temporal evolution of a circular grain embedded in anther grain. Time step = 1000 (a); 3000 (b); 5000 (c); and 7000 (d).

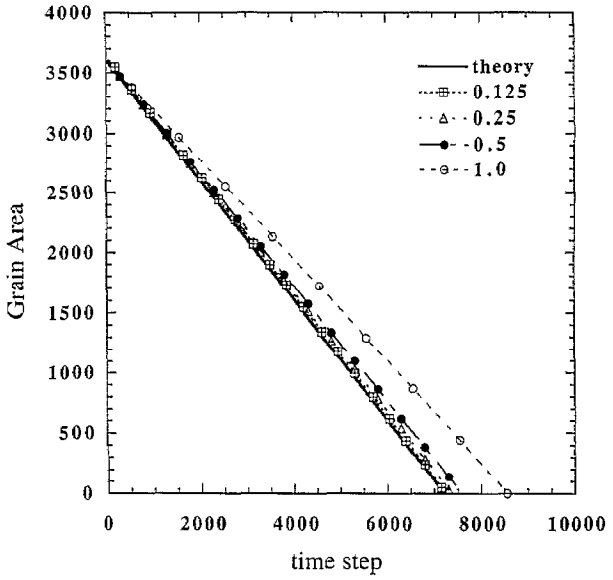


Fig. 2. The time dependence of the area of a circular grain in an infinite matrix. Comparing the analytical solution with simulations of $\mu = 0.125$, 0.25, 0.5 and 1.0.

The temporal evolution of a circular grain for $\mu = 1.0$ was shown in Fig. 1. It can be seen from Fig. 1 that the grain boundary is very smooth and circular at all times, indicating that no lattice anisotropy is introduced by discretizing the continuous Eq. (2). The time dependencies of grain areas for different values of $\mu$ are shown in Fig. 2. The solid line in Fig. 2 is the analytical solution described by Eq. (8). For all cases, the areas of the circular grain decrease linearly with respect to time, i.e. $R_0^2 - R_t^2 = kt$. Decreasing $\mu$ reduces $\Delta f_0$ and hence increases the width of the grain boundary according to Eq. (7). It is shown that a circular grain with a narrower boundary (Fig. 2) shrinks more slowly than that with a thicker boundary, i.e. the kinetic coefficient increases with the boundary width to a point. $k$ increases when $\mu$ decreases from 1.0 to 0.5, but remains constant when $\mu$ decreases further, e.g. from 0.25 to 0.125. It is clear that the grain boundary position and velocity differ significantly from those predicted by the sharp boundary approximation if there are insufficient grid points to resolve the boundary region (At $\mu = 1.0$ there are about five grid points in the grain boundary region). However, for $\mu = 0.125$, which corresponds to a grain boundary thickness of about ten grid points, the diffuse grain boundary model predicts positions and velocities that are identical to those predicted by the sharp-boundary solution. Therefore, if there are enough grid points to resolve a diffuse boundary, the migration velocity of a diffuse grain boundary is exactly the same

as that of a sharp grain boundary, even for a very small grain whose size is comparable to the grain boundary width.

## 4. Effect of grain boundary width on grain growth

To examine the effect of grain boundary width on grain growth in 2-D systems, we chose a 512 × 512 cell with 36 orientation field variables ($p = 36$). It has been shown that a large but finite number of orientation field variables is adequate to simulate grain growth kinetics [15]. We assumed the following numerical values for the parameters in the kinetic equations: $\alpha = 1.0$, $\beta = 1.0$, $\gamma = 1.0$ and $\kappa_i = 2.0$ and $L_i = 1.0$ for $i = 1-p$. The grid size along both Cartesian coordinate axes was chosen to be 2.0 and the time step for integration, $\Delta t = 0.25$. Periodic boundary conditions were applied. The simulations were initiated by assigning small random values to all field variables at every grid point, e.g. $-0.001 < \eta_i$ (for $i$) $< 0.001$, simulating a liquid. All kinetic data were obtained by averaging over several independent runs starting with similar initial conditions, but produced from a random number generator with different seed for the orientation field variables. Two cases, $\mu = 1.0$ and 0.125, were chosen to study the effect of grain boundary width on grain growth.

Microstructural evolution for $\mu = 1.0$ is shown in Fig. 3. Since the initial values for $\eta_i$'s are essentially zero, the very early stage of the simulation corresponds to nucleation and growth of a crystalline phase driven

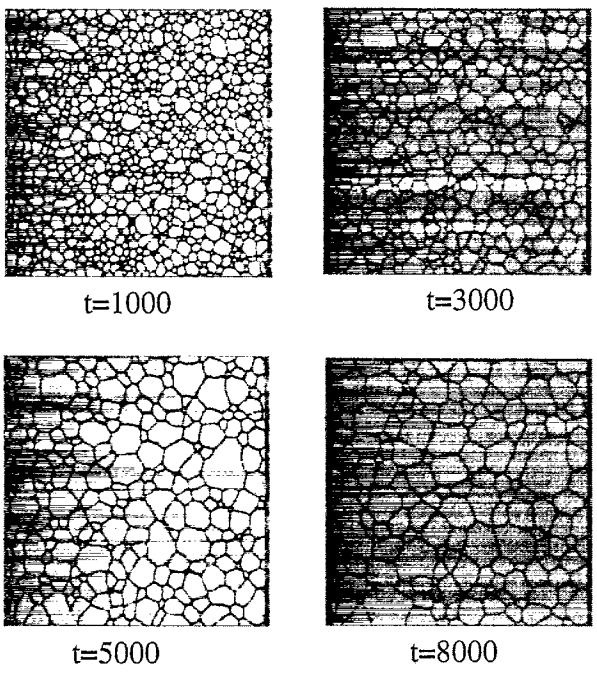


Fig. 3. The microstructural evolution in the 512 × 512 system with $\mu = 1.0$ and 36 orientation variables.

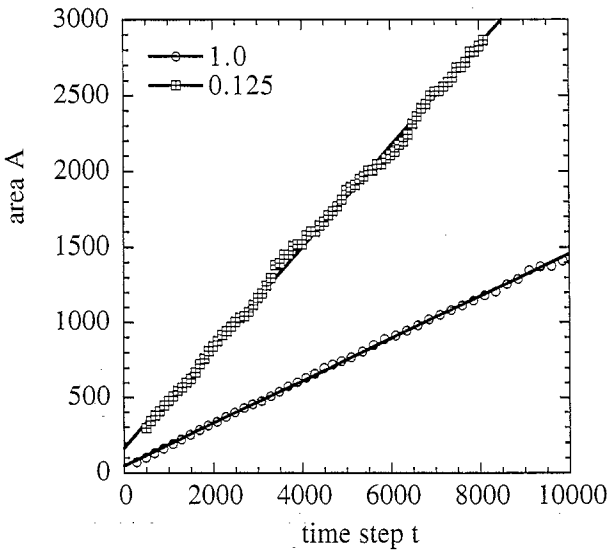


Fig. 4. The comparison of grain growth kinetics in the systems of $\mu = 1.0$ and 0.125. System size: 512 × 512, $p = 36$.

by the bulk free energy change. A well defined grain structure is formed after a short time, about 200 time steps, when the bulk driving force has been consumed. Further microstructure evolution is driven by the excess free energies associated with the grain boundaries, resulting in normal grain growth. The microstructure evolution for $\mu = 0.125$ is very similar to that of $\mu = 1.0$ (shown in Fig. 3). The transformation from a liquid to a grain structure takes longer time because smaller $\mu$ means less driven force for the transformation and there are fewer grains in the system after the transformation, a consequence of the larger grain boundary width. After the transformation, there are about 3000 grains in the $\mu = 1.0$ system and about 1000 grains in the $\mu = 0.125$ system.

The area of each grain at a given time step is calculated from the microstructure by counting the number of grid points within the grain. The average grain area at a given time step is then obtained by averaging over all the grains in a system. The average grain areas as a function of time for the $\mu = 0.125$ and 1.0 systems are plotted in Fig. 4. The average grain area increases linearly with time, indicating that the coarsening kinetics follows the power law $\bar{R}_t^m - \bar{R}_0^m = kt$ with the growth exponent $m = 2.0$, which is unaffected by varying the grain boundary width. However, the slopes of the two straight lines are different, which indicates that the kinetics coefficient $k$ varies as the grain boundary width changes from five to ten grid points. In this diffuse-interface field model, the grain boundary regions are defined as regions where the gradients $\nabla\eta_i$ are non zero. The curvature for a constant $\eta_i$ surface is given by the divergence of a unit normal vector to that surface [19,21], i.e. $\nabla \cdot \hat{n}$, where $\hat{n}$ is the unit vector normal to the surface. The $\nabla \cdot \hat{n}$ terms are equal to the

negative mean curvatures of surfaces and are implicitly included in the $\nabla^2\eta_i$ terms [19,21]. To accurately compute the $\nabla^2\eta_i$ and $\nabla\cdot\hat{n}$ terms numerically, there must be enough grid points to describe the grain boundary region. From Fig. 2, it can be seen that further refinement of grain boundaries will not change coarsening kinetics if there are enough grid points to resolve a diffuse boundary. Our simulations show that if there are more than seven grid points in grain boundary regions, the grain growth kinetics is almost independent of the grain boundary width in this model.

The grain size distributions in $\mu = 1.0$ and 0.125 systems are shown in Fig. 5 and the grain side (topological) distributions are compared in Fig. 6. The grain size distribution obtained from large scale Potts model simulations (E.A. Holm, private communication) is also included in Fig. 5. For a direct comparison, grain size distributions are normalized by their respective total areas under the curves. The grain size distributions in $\mu = 1.0$ and 0.125 systems are the same and almost identical with that of Potts model simulations. The topological distributions with different grain boundary widths are also quite similar (Fig. 6). The small fluctuation may come from the fact that there are fewer grains in the $\mu = 0.125$ system. In both cases, a peak is at the five sided grain, which is consistent with Potts model and soap froth [10–16]. Therefore, the grain size and topological distributions are independent of the grain boundary width even though the growth exponent $k$ changes as the grain boundary width varies from five to ten grid points.

To quantitatively compare the effect of grain boundary width on distributions, the $m$th moments of the side distribution are defined as:

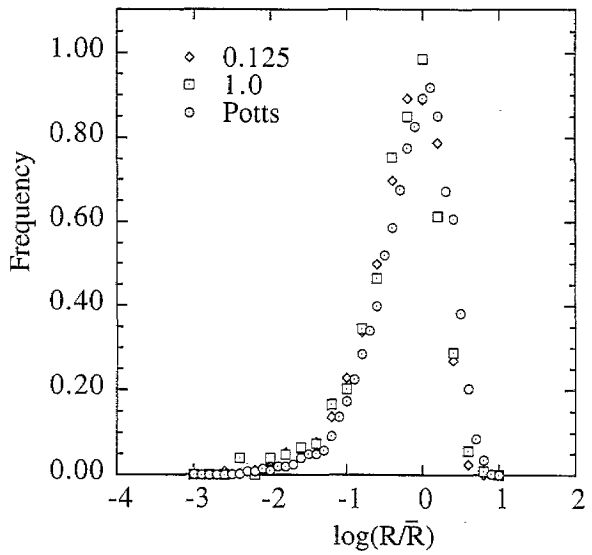


Fig. 5. The comparison of grain size distributions in $\mu = 0.125$ and $\mu = 1.0$ systems ($p = 36$) with Potts model simulation (E.A. Holm, private communication).

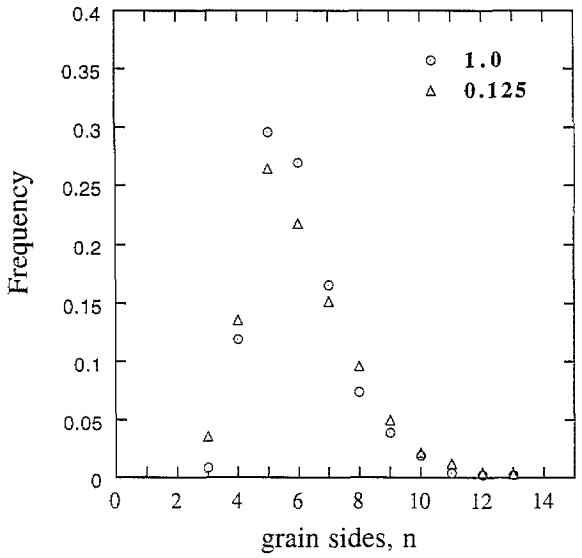


Fig. 6. The comparison of grain side distributions in systems $\mu = 1.0$ and 0.125.

$$\mu_m = \sum_{n=2}^{\infty} \rho(n)(n - \langle n \rangle)^m \tag{9}$$

where $\mu_m$ is the mth moment of the side distribution function $\rho(n)$ and $\langle n \rangle$ the average number of grain sides at a certain time and the absolute width of the side distribution is:

$$W = \sum_{n=2}^{\infty} \rho(n)(|n - \langle n \rangle|) \tag{10}$$

The average number of grain sides $\langle n \rangle$, obtained from this simulation is six, which is independent of grain boundary width and time in the scaling regime. The moment of the side distribution is an important indicator of the topological characteristics of a system during grain growth. Moments larger than $\mu_2$ are much more sensitive to the large-$n$ tail of the side distribution and to the measurement error and hence, normally they are only useful for qualitative analysis. The time dependence of the second moment $\mu_2$ is shown in Fig. 7. It can be seen that the $\mu_2$ value reaches the stable value $2.34 \pm 0.16$ after a very short time in the $\mu = 1.0$ system, indicating that the system has quickly reached the scaling regime. For the $\mu = 0.125$ system, the $\mu_2$ value is obviously larger than that of the $\mu = 1.0$ system before 3000 time steps and it reaches the stable value $2.34 \pm 0.16$ after the 4000 time steps. This indicates that the system with $\mu = 0.125$ approaches the scaling regime more slowly, which is the result of the less driving force in this system. It is interesting to see that the stable value of $\mu_2$ is identical in these two systems even though the grain boundary width is doubled. Therefore, it can be concluded that the lattice anisotropy associated with discretizing continuous equations is not a factor which affects the distributions in this model. The stable value

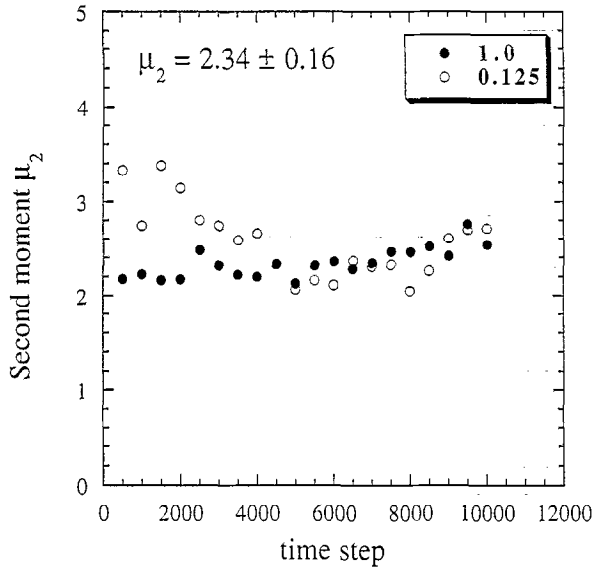


Fig. 7. The comparison of the second moment $\mu_2$ of the side distribution as the function of time for $\mu = 1.0$ and 0.125 systems.

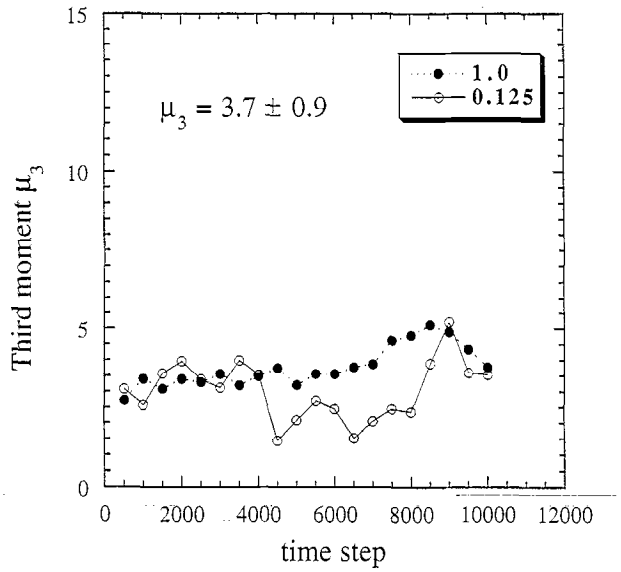


Fig. 9. The comparison of the third moment $\mu_3$ of the side distribution as the function of time for $\mu = 1.0$ and 0.125 systems.

of $\mu_2$ obtained from soap froth is $1.5 \pm 0.2$ [11] and is $2.4 \pm 0.1$ for Potts model simulations with the lattice anisotropy [10,11]. It is very interesting to notice that the $\mu_2$ value obtained from this model is closer to that of the Potts model than that of the soap froth.

The absolute widths, $W$, of side distributions are shown in Fig. 8. The dependence of the absolute width on time is similar to that of $\mu_2$. The stable value of $W$ is $1.1 \pm 0.1$ which is very close to the value of $W = 1.0 \pm 0.1$ for Potts model and $W = 1.1 \pm 0.3$ for the soap froth [11]. The absolute width of the side distribution is much less sensitive to many-sided grains. Hence, these three methods predict almost identical results.

The higher moments, $\mu_3$ and $\mu_4$, are plotted versus time in Figs. 9 and 10, respectively. It is clear that higher moments also reach the scaling-state values for both $\mu = 0.125$ and 1.0 systems. The stable value is $3.7 \pm 0.9$ for $\mu_3$ and is $26 \pm 5$ for $\mu_4$ in this model. The scaling-state value of $\mu_3$ obtained from Potts model is $5.25 \pm 1.25$ and is $1.0 \pm 0.5$ observed in the soap froth [11]. For the fourth moment ($\mu_4$), the stable value is $35 \pm 10$ from Potts model simulations and $6.0 \pm 3.6$ from the soap froth [11]. It can be seen that both values of $\mu_3$ and $\mu_4$ from this study are between those of the Potts model simulation and the soap froth. The larger values of high moments mean that many-sided grains have a

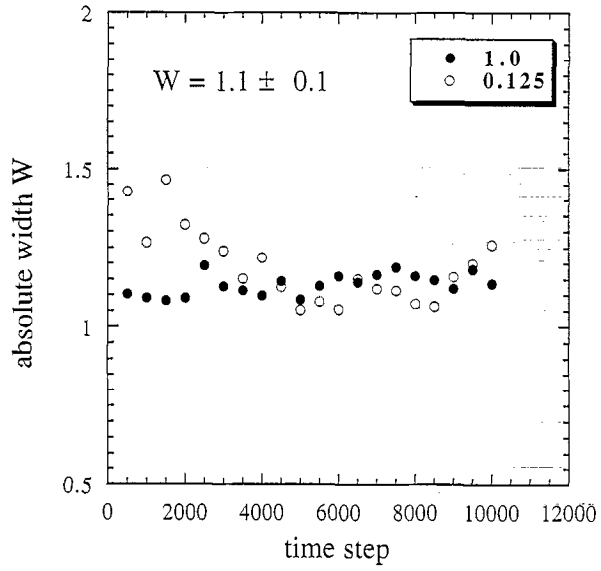


Fig. 8. The comparison of the absolute width $W$ of the side distribution as the function of time for $\mu = 1.0$ and 0.125 systems.

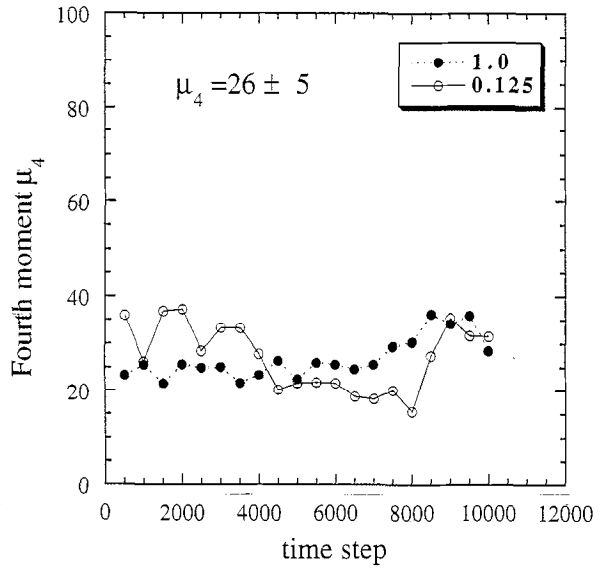


Fig. 10. The comparison of the fourth moment $\mu_4$ of the side distribution as the function of time for $\mu = 1.0$ and 0.125 systems.

higher frequency of occurrence in a system. Therefore, both simulations of this model and Potts model generate more many-sided grains than the soap froth does.

The tendency of generating more many-sided grains was attributed to the lattice anisotropy associated with the discrete lattice in the Potts model [10]. As the lattice anisotropy decreases in Potts model simulations, the moments of distributions approach to those of the soap froth [10]. However, it has been shown that the moments of sides distributions do not change with varying grain boundary width in this model and hence, the lattice anisotropy is not responsible for the generation of many-sided grains. We assert that some of many-sided grains come from the coalescence of neighboring grains of the same orientation, as only a finite number of orientation field variables was employed in simulations. It is the coalescence that contributes to the large-n tail of distributions and larger values of moments in this model than those of the soap froth. Coalescence also occurs in the finite $Q$ state Potts model simulations, which gives $\mu_3 = 5.25$ and $\mu_4 = 35$ [11] as stated above. In the Potts model it is shown that the moments drop to $\mu_3 = 1.7$ and $\mu_4 = 17$ when coalescence is totally prevented by using an infinitely degenerate system, however, lattice anisotropy was still high thus the moments are still not identical to those of the soap froth [10]. These values are even smaller than those obtained from this model ($\mu_3 = 3.7$ and $\mu_4 = 26$), in which there is no lattice anisotropy. Therefore, in addition to lattice anisotropy, coalescence is responsible for the discrepancies of distributions obtained from different methods. Finally, it should be pointed out that the phase-field model and the Potts model are more similar to the grain growth process in metals and ceramics, in which anisotropy and coalescence exist and the time for diffusion across grain boundaries is short compared to the diffusion along boundaries. While in the evolution of the soap froth, diffusion across boundaries is slower compared to the shape adjustment of bubbles.

## 5. Conclusions

We have shown that the grain growth kinetics will be slowed if there are insufficient grid points to resolve the grain boundaries in this diffuse-interface field model. When there are more then seven grid points in grain boundary regions, the grain growth kinetics is independent of the grain boundary width and the motion of a diffuse grain boundary is identical to its sharp-interface limit. The grain size distribution and topological distribution do not change with varying grain boundary width and they agree well with previous Potts model simulations. The moments of grain side distributions reach stable values in the scaling regime and they are independent of the grain boundary width. The coalescence of grains affects the topological distributions.

## Acknowledgements

D.F. and S.P.C.'s work is supported by the US Department of Energy and L.-Q.C.'s work is supported by the National Science Foundation under the grant number DMR 96-33719 and the simulations were performed at the Pittsburgh Supercomputing Center and the Advanced Computing Laboratory at Los Alamos National Laboratory.

## References

[1] H.V. Atkinson, Acta Metall. 36 (1988) 469.
[2] J.A. Glazier, Phil. Mag. B62 (1990) 615.
[3] V.E. Fradkov, Physica D: Nonlinear Phenomena 66 (1993) 50.
[4] M.P. Anderson, D.J. Srolovitz, G.S. Grest, P.S. Sahni, Acta Metall. 32 (1984) 783.
[5] D.J. Srolovitz, M.P. Anderson, P.S. Sahni, G.S. Grest, Acta Metall. 32 (1984) 793.
[6] M.P. Anderson, G.S. Grest, Phil. Mag. B59 (1989) 293.
[7] J.A. Glazier, M.P. Anderson, G.S. Grest, Phil. Mag. B62 (1990) 615.
[8] G.S. Grest, D.J. Srolovitz, M.P. Anderson, Phys. Rev. B38 (1988) 4752.
[9] G.S. Grest, D.J. Srolovitz, M.P. Anderson, Acta Metall. 33 (1985) 509.
[10] E.A. Holm, J.A. Glazier, D.J. Srolovitz, G.S. Grest, Phys. Rev. A43 (1991) 2662.
[11] J.A. Glazier, M.P. Anderson, G.S. Grest, Phil. Mag. B62 (1990) 615.
[12] J.A. Glazier, J. Stavans, Phys. Rev. A40 (1989) 7398.
[13] J. Stavans, J.A. Glazier, Phys. Rev. Lett. 62 (1989) 1318.
[14] D. Weaire, F. Bolton, Phys. Rev. Lett. 65 (1990) 3449.
[15] Danan Fan, L.-Q. Chen, Acta Mater. 45 (1997) 611.
[16] Danan Fan, L.-Q. Chen, Acta Mater. 45 (1997) 1115.
[17] L.-Q. Chen, Scr. Metall. et Mater. 32 (1995) 115.
[18] L.-Q. Chen, W. Yang, Phys. Rev. B50 (15) (1994) 752.
[19] S.M. Allen, J.W. Cahn, Acta Metall. 27 (1979) 1085.
[20] Danan Fan, PhD Dissertation, The Pennsylvania State University, PA, 1996, pp. 69–73.
[21] J.W. Cahn, J.E. Hilliard, J. Chem. Phys. 28 (1958) 258.
[22] Danan Fan, L.-Q. Chen, Phil. Mag. Lett. 75 (1997) 187.